Received: 13 May 2022 | Revised: 11 September 2022 | Accepted: 14 September 2022

DOI: 10.1002/jbm.a.37449

RESEARCH ARTICLE

Measuring dimensionality of cell-scaffold contacts of primary human bone marrow stromal cells cultured on electrospun fiber scaffolds

Stephanie J. Florczyk[1] | Nathan A. Hotaling[1,2] | Mylene Simon[3] | Joe Chalfoun[3] | Allison L. Horenberg[1] | Nicholas J. Schaub[1,2] | Dongbo Wang[1] | Piotr M. Szczypiński[4] | Veronica L. DeFelice[5] | Peter Bajcsy[3] | Carl G. Simon Jr[1]

[1]Biosystems and Biomaterials Division, National Institute of Standards and Technology, Gaithersburg, Maryland, USA

[2]Axle Informatics, Rockville, Maryland, USA

[3]Software and Systems Division, National Institute of Standards and Technology, Gaithersburg, Maryland, USA

[4]Institute of Electronics, Lodz University of Technology, Lodz, Poland

[5]Biochemistry and Molecular Biology Program, Georgetown University, Washington, District of Columbia, USA

Correspondence
Peter Bajcsy, Software and Systems Division, National Institute of Standards and Technology, Gaithersburg, MD, 20899, USA.
Email: peter.bajcsy@nist.gov

Carl G. Simon, Jr., Biosystems and Biomaterials Division, National Institute of Standards and Technology, Gaithersburg, MD, USA.
Email: carl.simon@nist.gov

Abstract

The properties and structure of the cellular microenvironment can influence cell behavior. Sites of cell adhesion to the extracellular matrix (ECM) initiate intracellular signaling that directs cell functions such as proliferation, differentiation, and apoptosis. Electrospun fibers mimic the fibrous nature of native ECM proteins and cell culture in fibers affects cell shape and dimensionality, which can drive specific functions, such as the osteogenic differentiation of primary human bone marrow stromal cells (hBMSCs), by. In order to probe how scaffolds affect cell shape and behavior, cell-fiber contacts were imaged to assess their shape and dimensionality through a novel approach. Fluorescent polymeric fiber scaffolds were made so that they could be imaged by confocal fluorescence microscopy. Fluorescent polymer films were made as a planar control. hBSMCs were cultured on the fluorescent substrates and the cells and substrates were imaged. Two different image analysis approaches, one having geometrical assumptions and the other having statistical assumptions, were used to analyze the 3D structure of cell-scaffold contacts. The cells cultured in scaffolds contacted the fibers in multiple planes over the surface of the cell, while the cells cultured on films had contacts confined to the bottom surface of the cell. Shape metric analysis indicated that cell-fiber contacts had greater dimensionality and greater 3D character than the cell-film contacts. These results suggest that cell adhesion site-initiated signaling could emanate from multiple planes over the cell surface during culture in fibers, as opposed to emanating only from the cell's basal surface during culture on planar surfaces.

KEYWORDS
bone marrow stromal cell, cell morphology, cell-material interactions, tissue engineering, tissue scaffold

Stephanie J. Florczyk and Nathan A. Hotaling contributed equally to this work.

1 | INTRODUCTION

Cells in vivo reside within a niche that is comprised of a 3D matrix of extracellular matrix (ECM) proteins.[1] These ECM proteins can interact with a cell through specific and non-specific cellular adhesion sites. Cell adhesion may stimulate intracellular biochemical signaling events that originate from the site of adhesion and permeate into the cell.[2–5] The interaction of the cell with its microenvironment can affect the behavior of the cell[6] and may induce the cell to undergo functions such as proliferation, differentiation, or apoptosis.

Primary human bone marrow stromal cells (hBMSCs) are adult-derived progenitor cells that have potential for clinical use in musculoskeletal indications such as tissue-engineered bone, cartilage, and marrow.[7] Tissue engineering scaffolds are often used as templates for 3D cell culture providing an artificial niche to support and guide cell function. The physical properties of the cell niche, such as its structure, chemistry and mechanical properties play a role in directing cell function. Electrospun fiber-based scaffolds have been advanced for tissue engineering since they mimic the fibrous structure of native ECM, such as collagen, elastin, and fibronectin. Culture of hBMSCs in fiber-based scaffolds drives them toward an osteogenic-like lineage where they express osteogenic proteins and build a bone-like matrix.[8,9]

The mechanism whereby fiber-based scaffolds induce hBMSCs toward osteogenesis may include cell morphological cues.[10–12] The cell niche in which the cells reside may physically guide the cells into morphologies that support differentiation.[13] Cells cultured in 3D scaffolds may adopt morphologies with greater 3D character than during culture on flat substrates, where the cells typically assume a flattened or planar shape.[14,15] The scaffold can affect the size and geometry of the contact area with the cell, which can affect the formation of focal adhesions and the initiation of outside-in signaling events.[16,17] In addition, cells in fiber-based scaffolds may extend along fibers and take on elongated morphologies that differ from the lower aspect ratio morphologies observed on planar substrates.

The change in cell shape may be reflected in the shape of intracellular organelles, whose function can be influenced by shape changes.[18,19] The altered organelle structure may modulate biochemical signaling to drive an osteogenic response. Changes to cell shape may also affect the shape of the nucleus, causing changes in the structure of gene promoters and chromatin that influence gene expression.[20–22]

Cell shape changes may affect cell volume and dimensionality, which affect the concentration and diffusion of signaling molecules and the distances that signaling molecules must travel to reach their destination within the cell.[23,24] Meyers et al.[25] showed that signaling molecules that emanate from the cell membrane will permeate the cell volume more rapidly when a cell is thinner, since the intracellular spaces are within closer proximity to the membrane. Likewise, Rangamani et al.[26] demonstrated that signaling from the cytoplasm to the membrane can establish molecular gradients within the membrane of cells that have elongated, higher-aspect ratio shapes. The changes in cell shape and dimensionality that affect signaling kinetics may ultimately affect cell function.

In order to assess how cells interact with the microenvironment, we have examined the 3D shape and dimensionality of cell-scaffold contacts during culture in fiber-based scaffolds and on planar surfaces. We hypothesized that when cells are cultured on flat surfaces, their adhesion sites ought to be contained to a plane along the bottom of the cell. Further, we hypothesized that in 3D scaffolds, cell-scaffold adhesion sites should occur along multiple planes that create a 3D point cloud that occupies a volume.

In order to assess cell-scaffold contacts, fluorescent scaffolds were used for cell culture so that confocal fluorescence microscopy could be used to simultaneously image fluorescently stained cells and the fluorescent scaffold within which the cells were cultured. Fiber-based scaffolds were made by electrospinning and flat polymer films were made by spin-coating. Scaffolds and films were made from the same polymer, poly(lactic-co-glycolic acid) (PLGA), so that the effects of material chemistry on cell behavior would be minimized. The scaffolds and films were rendered fluorescent by spiking them with a fluorophore that was conjugated to PLGA. By using a fluor conjugated to PLGA, the solubility and release of the fluor in cell culture medium was reduced. The cells and the scaffolds were imaged by confocal fluorescence microscopy and 3D image analysis was used to measure the shape and dimensionality of the cells and the cell-scaffold contacts.

2 | MATERIALS AND METHODS

2.1 | Preparation of spuncoat films and electrospun fibers

Three types of substrates were used for this study: (i) electrospun PLGA fibers with a large fiber diameter of 2.6 μm (MF), (ii) electrospun PLGA fibers with a medium fiber diameter of 1.1 μm (MMF) and (iii) flat spuncoat PLGA films (SC). All substrates were prepared from a 90:10 blend by mass of PLGA:PLGA-FKR648 (PLGA 50:50 molar ratio of L to G, relative molecular mass ≈110,000 g/mol, Lactel Absorbable Polymers; PLGA-FKR648, PLGA 50:50 molar ratio of L to G, relative molecular mass ≈25,000 g/mol, Flamma Fluor FKR648 ester-linked to the PLGA, Akina Inc., Polyscitech). The fluorescent PLGA-FKR648 was blended with PLGA so that substrates could be imaged by fluorescence microscopy. The Flamma Fluor in PLGA-FKR648 was covalently linked to the PLGA so that it would not leach out of the polymer substrates into the cell culture medium.

For MF scaffolds, the PLGA:PLGA-FKR648 blend was dissolved in 3:1 acetone: ethyl acetate at 260 mg/ml and electrospun (18 gauge steel needle, 2.3 ml/h, tip to collector distance of 15 cm, 14 kV, high voltage generator, ES30P-5 W, Gamma High Voltage Research) onto an aluminum foil target. MMF scaffolds were electrospun by the same approach with the following modifications: 260 mg/ml in acetone solvent, 22 ga. steel needle, 1.25 ml/h, and 12 kV. After electrospinning, nonwoven MF and MMF fiber mats were lifted off of the aluminum foil and wrapped around 12 mm diameter glass coverslips. A tiny dab

of acetone was used to "glue" the fiber mats to the coverslips to keep them in place.

For SC films, the 90:10 PLGA:PLGA-FKR648 blend was dissolved in acetone at a concentration of 21% (mass/volume) and spuncoat (0.1 ml, 2000 rpm, 60 s) on glass cover slips (12 mm in dia.).

MF, MMF, and SC samples on glass coverslips were affixed to the bottoms of the wells in a 24-well plate with silicone vacuum grease. The 24-well plates with samples were sterilized with ethylene oxide (Andersen Products, Haw River, NC) for 12 h and then degassed for 2 days under house vacuum. Prior to cell seeding, the scaffolds were incubated in complete medium (0.5 ml/well) in a humidified incubator at 37°C with 5% (by volume) CO_2 for 2 days.

2.2 | Substrate characterization

Scanning electron microscopy (SEM) was used to image MF and MMF substrates and to determine fiber diameter (Figure 1). For SEM, MF and MMF were removed from the aluminum foil after electrospinning, cut into 5 mm × 5 mm squares and mounted on SEM stubs using carbon conductive double-sided tape. MF and MMF were sputter-coated with gold and imaged (3 kV, 6.5 μA, S-4700eII FE-SEM, Hitachi). Seven (MF) or eight (MMF) SEM images were captured of the fiber samples which were analyzed to determine fiber diameter using the DiameterJ plugin for ImageJ.[27] DiameterJ determines the diameter at every centerline pixel along each fiber in an SEM image to generate thousands of data points for constructing a histogram of fiber diameter.

Atomic force microscopy (AFM) was used to measure the surface roughness of SC films (Dimension Icon, Bruker) using a Bruker ScanAsyst-Air tip (resonant frequency 70 kHz, spring constant 0.4 N/m, length 115 μm, width 25 μm) (Figure 1). Six scans of 50 μm by 50 μm (512 samples/line, 512 lines, 0.977 Hz scan rate) were used to calculate a root mean square roughness (RMS). Samples were imaged using PeakForce tapping to assess surface topography.

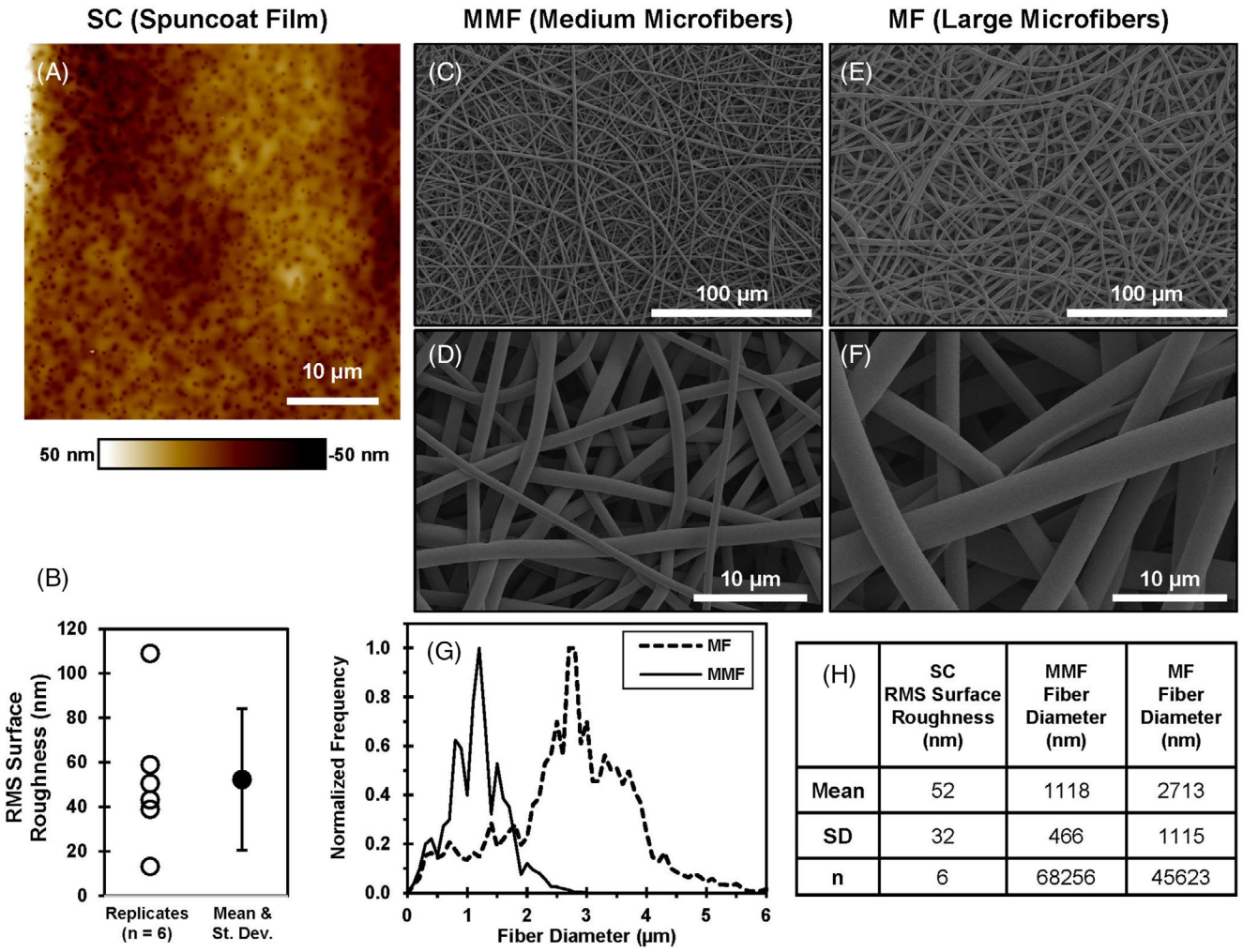

FIGURE 1 Structural characterization of substrates. (A) Atomic force microscopy (AFM) topography image of SC film with height scale below. (B) Root mean square surface roughness (RMS) measurements of SC films from AFM. (C and D) Scanning electron microscopy (SEM) of MMF. (E and F) SEM of MF. (G) Histograms of fiber diameter measurements for MMF and MF. (H) Mean RMS surface roughness for SC and mean fiber diameter for MMF and MF

2.3 | Cell culture

Primary hBMSCs (Tulane Center for Gene Therapy, donor #8004 L, 22 year. male, iliac crest, collected by informed consent, used with appropriate permissions by review of the NIST Institutional Review Board) were cultured in medium (α-MEM containing 16.5% by volume fetal bovine serum, 4 mmol/L L-glutamine, and 100 units/ml penicillin and 100 μg/ml streptomycin) in a humidified incubator (37°C with 5% CO_2 by volume) to 70% confluency and trypsinized (0.25% trypsin by mass containing 1 mmol/L ethylenediaminetetraacetate [EDTA], Invitrogen). hBMSCs at passage four were seeded onto substrates in 24-well plates by adding 1 ml of cell culture medium containing 2500 cells to each well (1250 cells/cm^2). Cells were cultured on substrates for 24 h which enabled them to achieve a stable morphology.

2.4 | Confocal microscopy

After 24 h culture, cells on samples were fixed with 3.7% by volume formaldehyde in Dulbecco's phosphate buffered saline (D-PBS, Life Technologies) for 1 h at room temperature, washed three times with D-PBS, permeabilized with 0.1% by volume Triton X-100 for 10 min, washed three times with D-PBS, stained with OregonGreen-Maleimide 488 (5 μmol/L in D-PBS, Life Technologies) for 1 h at room temperature, washed three times with D-PBS, stained with 4′,6-diamidino-2-phenylindole, dihydrochloride (DAPI, 0.03 mmol/L in D-PBS, Life Technologies) for 5 min, washed three times with D-PBS and stored in D-PBS at 4°C until imaged.

For imaging, the samples were immersed in D-PBS and imaged with a confocal laser scanning microscope (Leica SP5 II confocal microscope, Leica Microsystems) using a 63× water immersion objective (0.9 numerical aperture). Z-stacks of images (voxel dimensions of 120 nm × 120 nm × 462 nm, 1 Airy unit, line average 3, 400 Hz) of hBMSCs were captured for each substrate type on two channels: (1) cell membrane green fluorescence (OregonGreen Maleimide 488, excitation 488 nm, emission 501–570 nm) and (2) substrate red fluorescence (Flamma Fluor FKR648, excitation 633 nm, emission 652–708 nm). In addition, a single image (not a Z-stack) was captured for each substrate on 1 channel: cell nucleus blue fluorescence (DAPI, excitation 405 nm, emission 413–467 nm). The cell nucleus blue fluorescence image was used to confirm that each object that was imaged via Z-stacking on the green and red channels (i) had only a single nucleus, (ii) was a single cell, and (iii) was not a cluster of multiple cells. The nucleus channel was not analyzed for any shape metrics. Each Z-frame in the Z-stacks was exported as an 8 MB monochrome tif image (16 bits per pixel) with a size of 2048 × 2048 pixels (246 μm × 246 μm). Each Z-stack was between 923 MB and 1468 MB (2048 pixels [X] × 2048 pixels [Y] × 110 to 175 pixels [Z]). As determined from calculations based on the lateral and axial Rayleigh criterion equations, the lateral and axial limits of resolution for this system are 277 nm and 1228 nm for OregonGreen Maleimide, and 359 nm and 1593 nm for Flamma Fluor FKR648.[28]

Cells near the middle of substrates and away from substrate edges were selected for imaging to reduce edge effects and to assure that imaged cells were only in contact with the material (SC, MMF, MF) and not touching the glass coverslips. Only individual hBMSCs that were not touching other cells (one nucleus per object) were imaged, so that the observed cell morphologies were influenced primarily by the substrates and not by interactions with other cells. During image captures, cells were centered in the field of view so that cells were not touching the edges of the images to enable accurate analysis of single-cell shape. A total of 414 cells were imaged where greater than one hundred cells were imaged for each scaffold type as summarized in Table 1. The full data set consisted of 125,230 Z-frame images and 1.04 TB of data.

TABLE 1 Summary of confocal Z-stacks used for analysis

Treatments	# of Z-stacks captured	# of Z-stacks used in analysis		
		Cells	Geom	Stats
SC	165	165	160	48
MMF	114	114	107	110
MF	135	135	120	101
Total	414	414	387	259

2.5 | Image analysis

The descriptions of development and testing of the algorithms used for 3D image analysis were published separately so that they could be described in detail.[29,30] First, algorithms for segmenting the cell and scaffold channels into foreground and background were developed and tested using a variety of methods to verify results. Second, the best-performing methods were used to produce the final segmentations for the cells and scaffolds. Third, a method for determining cell-scaffold contacts was developed to identify the locations where the cells were touching the scaffolds. Fourth, shape metrics were determined for the cells and cell-scaffold contacts. Although, the image analysis process is summarized below and in Figure 2, the primary focus of the current article is to discuss the shape metrics for cells and cell-scaffold contacts.

2.5.1 | Cell segmentation

The 414 3D cell Z-stacks (OregonGreen Maleimide 488 channel) were segmented to isolate the cell (foreground) from the background. In previous work, six cell segmentation algorithms were developed and compared to human manual segmentations.[30] The best-performing algorithm had an average 3D segmentation accuracy of 84% (Dice score of 0.84 on scale of 0–1), as measured by the Dice similarity index. An adaptation of the best performing algorithm was used to segment cells in the current data set[29] and key steps include: smoothing by morphological erosion and dilation in XY directions; segmenting cells using minimum error threshold optimization; removing objects touching image edges (cannot measure objects that are cutoff); and

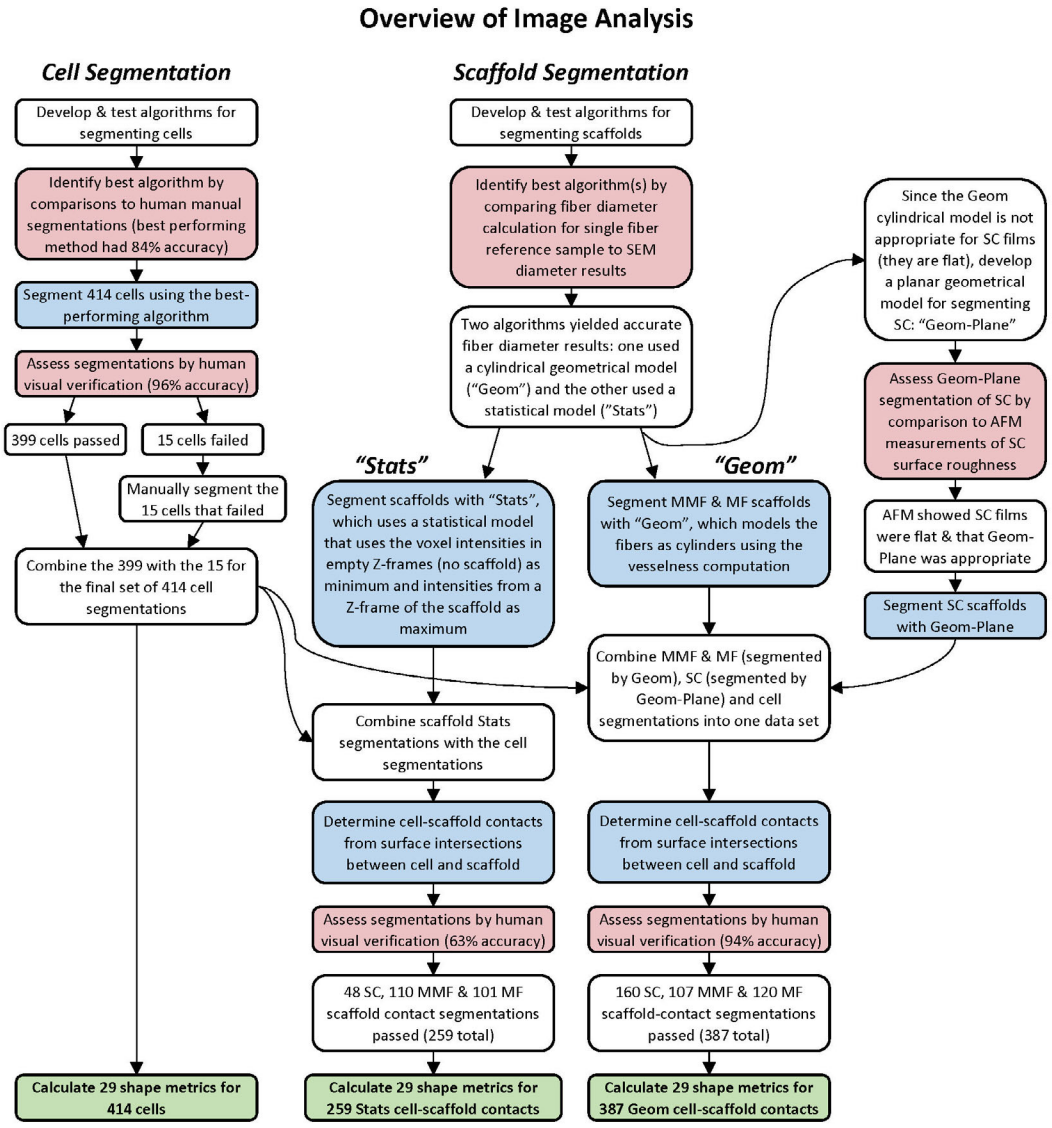

FIGURE 2 Overview of image analysis and computational methods for cell and scaffold segmentation and for determining cell-scaffold contacts. Red boxes indicate points of assessment and verification. There were six segmentations indicated by blue boxes. Green boxes are the end points. AFM, atomic force microscopy; MMF, medium microfiber (nominal fiber diameter 1.1 μm); MF, microfiber (nominal fiber diameter 2.7 μm); SEM, scanning electron microscopy; SC, spun-coat films

finding the largest object and removing all others (assumes that cell is a single object). Cell segmentations were visually inspected to assess accuracy, segmentation accuracy was 96% (399 out of 414) and 15 that were deemed inadequate were segmented manually.[31]

2.5.2 | Scaffold segmentation

In previous work, eight algorithms for segmenting scaffolds were developed[29] and tested using a reference single-fiber sample. The reference sample allowed the same fiber to be analyzed by SEM and confocal fluorescence microscopy. SEM has better resolution and can serve as a reference measurement for confocal. Using a brief electrospinning time and the same polymers and solvents as described above, a single fluorescent fiber was electrospun across a span. The fiber was imaged by SEM and fiber diameter was determined in the SEM micrographs using a validated algorithm called DiameterJ.[27] The exact same fiber was also imaged by 3D confocal fluorescence microscopy, the Z-stacks were segmented by the eight test algorithms and fiber diameter was determined from the segmented images. Two of the algorithms yielded accurate measurements of fiber diameter,[29] so both were used to analyze the scaffold Z-stacks in order to improve confidence in the results. One algorithm used a geometric model ("Geom") where MF and MMF were modeled as cylinders. The other algorithm used a statistical model ("Stats") where voxel intensities were modeled as probabilities for segmenting them as scaffold or background.

"Geom" scaffold segmentation for MMF and MF

MMF and MF scaffolds were segmented using a geometrical model ("Geom") with a modified Frangi's vesselness computation to model the fibers as cylinders.[29] The modification limited the enhancement effect to fibers arranged horizontally in relation to the scaffold surface, and at the same time it reduced vertical blurring artifacts introduced by the confocal microscopy imaging. The vesselness computation followed greyscale thresholding at approximately 8% (20/256).

"Geom" scaffold segmentation for SC

Since SC films are flat and cannot be modeled by cylinders, SC films were geometrically modeled by a plane. AFM showed SC surface roughness was 52 nm (Figure 1), which is nine-times smaller than the Z-depth of confocal voxels (462 nm), and confirms that a planar model is appropriate. Planes were determined for SC scaffold voxel intensities (normalized to the maximum value) using a weighted least-squares fit.[29]

"Stats" scaffold segmentation

The statistical probability model ("Stats") computed a probability that a voxel is either scaffold or background in each Z-stack. A Z-frame at the top or bottom of each stack, that had no scaffold voxels, and was primarily background, was used to determine the background for each Z-stack. The maximum intensity from each Z-stack was used as the maximum value for scaffold. The midpoint between the background and the maximum was used as the threshold for labeling each voxel in the stack as either scaffold (≥0.5) or background (<0.5).[29]

2.5.3 | Determining cell-scaffold contacts

Geom: The segmented cell Z-stacks and Geom-segmented scaffold Z-stacks were combined into a two-channel Z-stack. Cell-scaffold contacts were determined as (i) a co-occurrence of or (ii) a one voxel adjacency of cell and scaffold voxels.

Stats: The segmented cell Z-stacks and Stats-segmented scaffold Z-stacks were combined into a two-channel Z-stack. Cell-scaffold contacts were determined as (i) a co-occurrence of or (ii) a one voxel adjacency of cell and scaffold voxels.

2.5.4 | Visual verification

The cell segmentations and the cell-scaffold contact segmentations were assessed visually by three experts to verify accuracy.[31] A web interface was constructed where maximum intensity projection images were created for each cell as viewed down each of the three major axes (X, Y, Z). For each of the cell-scaffold contact segmentations, 3D movies were created of the Z-stacks rotating on their X and Y axes for three combinations of channels: (i) cell + scaffold + cell-scaffold contacts, (ii) scaffold + contacts, and (iii) contacts. The images and movies can be viewed at the data link.[31] The accuracy of the segmentations was visually verified by three experts using a qualitative scoring system and determined to be 96% accurate for cell segmentations, 94% accurate for the cell-scaffold contacts for the Geom model and 63% accurate for the cell-scaffold contacts for the Stats model.[29]

2.6 | Calculating shape metrics

Twenty-nine shape metrics (summarized in Table S1) each were computed for (i) the cell segmentations ($n = 414$), (ii) the Geom cell-scaffold contacts ($n = 387$), and (iii) the Stats cell-scaffold contacts ($n = 259$). Discussion of these shape metrics is the primary focus of this current manuscript.

The primary goal of this study was to assess the dimensionality of the cell-scaffold contacts. Dimensionality can be defined as "the quality of having height, length, and width rather than being flat" (https://dictionary.cambridge.org). Using this definition, measures of an object's flatness or 3Dness will be related to the dimensionality. Herein, the key metrics for assessing shape dimensionality are "L_1-Depth" and "Sqrt(L_1)." These metrics are determined by fitting a 3D point cloud with a gyration tensor which yields a best-fit ellipsoid.[14,15] For fibers (MMF and MF), the cell-scaffold contact may be multiple objects that are not in contact with one another, since the cell may be in contact with many fibers that are not touching. The gyration tensor was fit to all the contact objects for a given cell as if they were one object, as if the contacts were connected to one another in 3D space with struts that had no mass. L_1-Depth is the caliper length of the object along the L_1-axis, which is the shortest axis of the best-fit ellipsoid. L_2-axis is the middle length axis and L_3-axis is the longest axis. L_1-Depth is a measure of dimensionality, since the shortest axis of an object with greater 3D character will be longer than the shortest axis of flatter objects.[15] In other words, flatter objects have a shorter short axis (smaller L_1-Depth) and more 3D objects have a longer short axis (larger L_1-Depth).

Sqrt(L_1) is the square root of the shortest principal moment of the gyration tensor, which is also the length of the shortest radius of the best fit ellipsoid. As with L_1-Depth, a larger Sqrt(L_1) indicates greater dimensionality and a more 3D shape (less flat).

Sqrt(L_1) and L_1-Depth are related to one another, but they are calculated differently and may not always correlate with one another. For example, if an object had fine, thin structures that extended far away from the object's centroid, then the L_1-Depth could be much larger than the Sqrt(L_1). This is because the Sqrt(L_1) comes from the gyration tensor which is derived from the gyrational momentum that occurs when an object is rotated about an axis. Fine, thin structures may not have a large effect on the gyration tensor if they do not represent a significant fraction of the object's mass. In contrast, L_1-Depth may be more greatly affected by thin, fine structures that extend away from the centroid of an object. This is because L_1-Depth is a caliper length, as if a set of calipers were closing down on the object, and any extensions off the surface of the object, even if they are fine and thin, will stop the calipers resulting in a larger caliper length. It is useful to consider both metrics, L_1-Depth and Sqrt(L_1), since they provide related but different perspectives on the attribute of dimensionality.

2.7 | Visualizations

Three dimensional (3D) visualizations of cells, scaffold and cell-scaffold contacts were created using Imaris Viewer 9.8 (Build 59,780 for x64, 2021). 3D visualizations of ellipsoids were created using Autodesk Inventor Professional 2021 (Build 183, 64-bit Edition).

2.8 | Statistical analysis

Statistical analysis was conducted in Matlab R2021b (Update 1, 9.11.0.1809720) using the Anderson-Darling test for normality (`adtest`), the Kruskal-Wallis test for non-normal data (`kruskalwallis`), and the Dunn's pairwise test for non-normal data with Sidak's correction for multiple comparisons [`multcompare(stats1, "CType", "dunn-sidak")`].

2.9 | Data deployment

Data are available for download for further analysis: raw images, segmented images, and movies for visual verification.[32] In addition, a Supplemental File S1 has been included for the current article and has the results for the 29 shape metrics for the cells, Geom cell-scaffold contacts and Stats cell-scaffold contacts.

3 | RESULTS

SEM was used to assess the fiber diameter of the MMF and MF scaffolds (Figure 1). The mean fiber diameter was 1.1 μm (standard deviation [SD] 0.5 μm) for MMF and 2.7 μm (SD 1.1 μm) for MF. AFM was used to assess the surface roughness of the SC films. The RMS

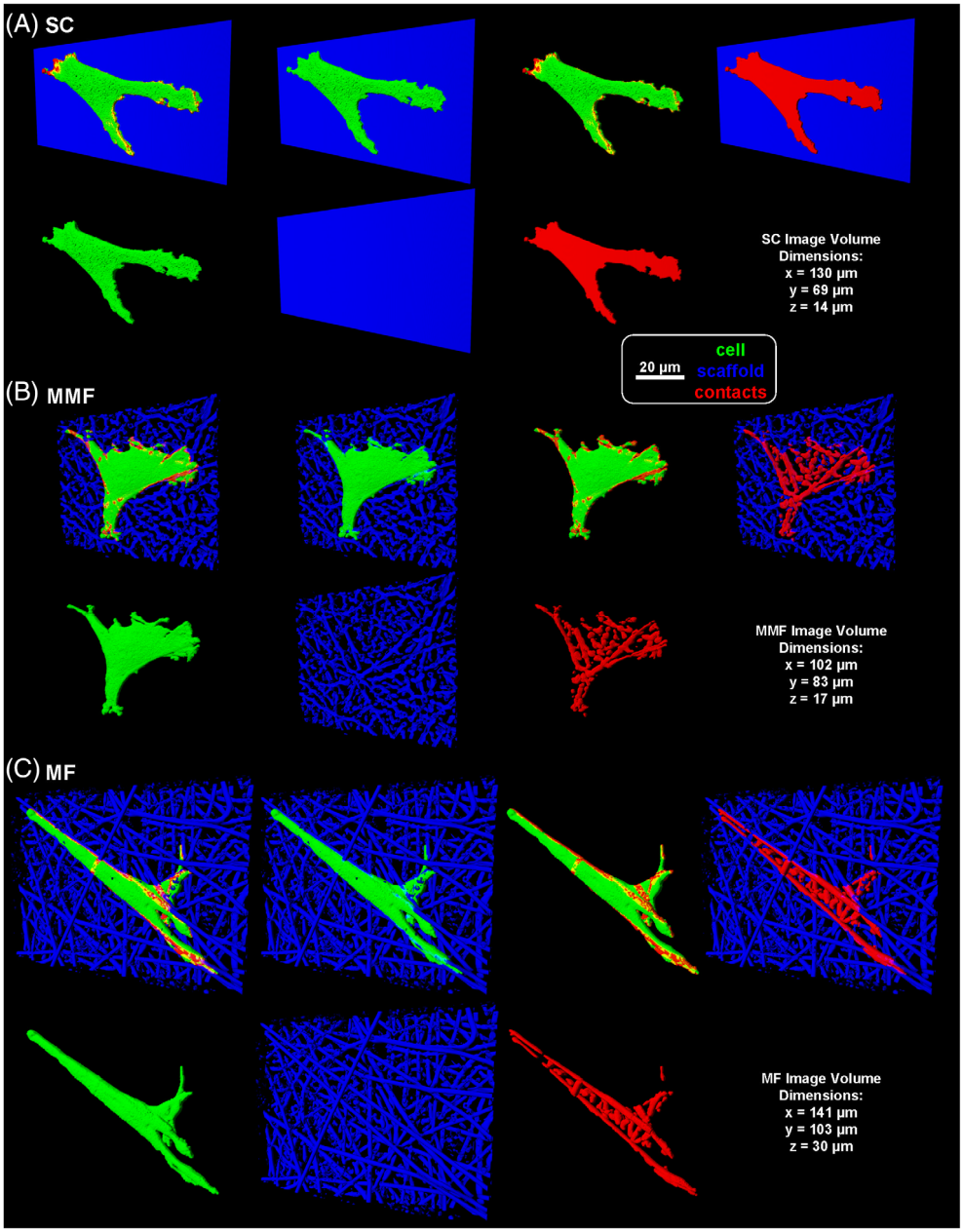

FIGURE 3 3D renderings of cells, scaffolds, and cell-scaffold contacts (Geom analysis). Cells and scaffolds were imaged by confocal fluorescence microscopy and segmented to generate the "cell" (green) and "scaffold" (blue) channels. The cell and scaffold channels were analyzed to determine regions where they were in contact ("contacts," red). All seven combinations of the three channels are shown for each of the three treatments (SC, MMF, MF). The scale bar applies to all images

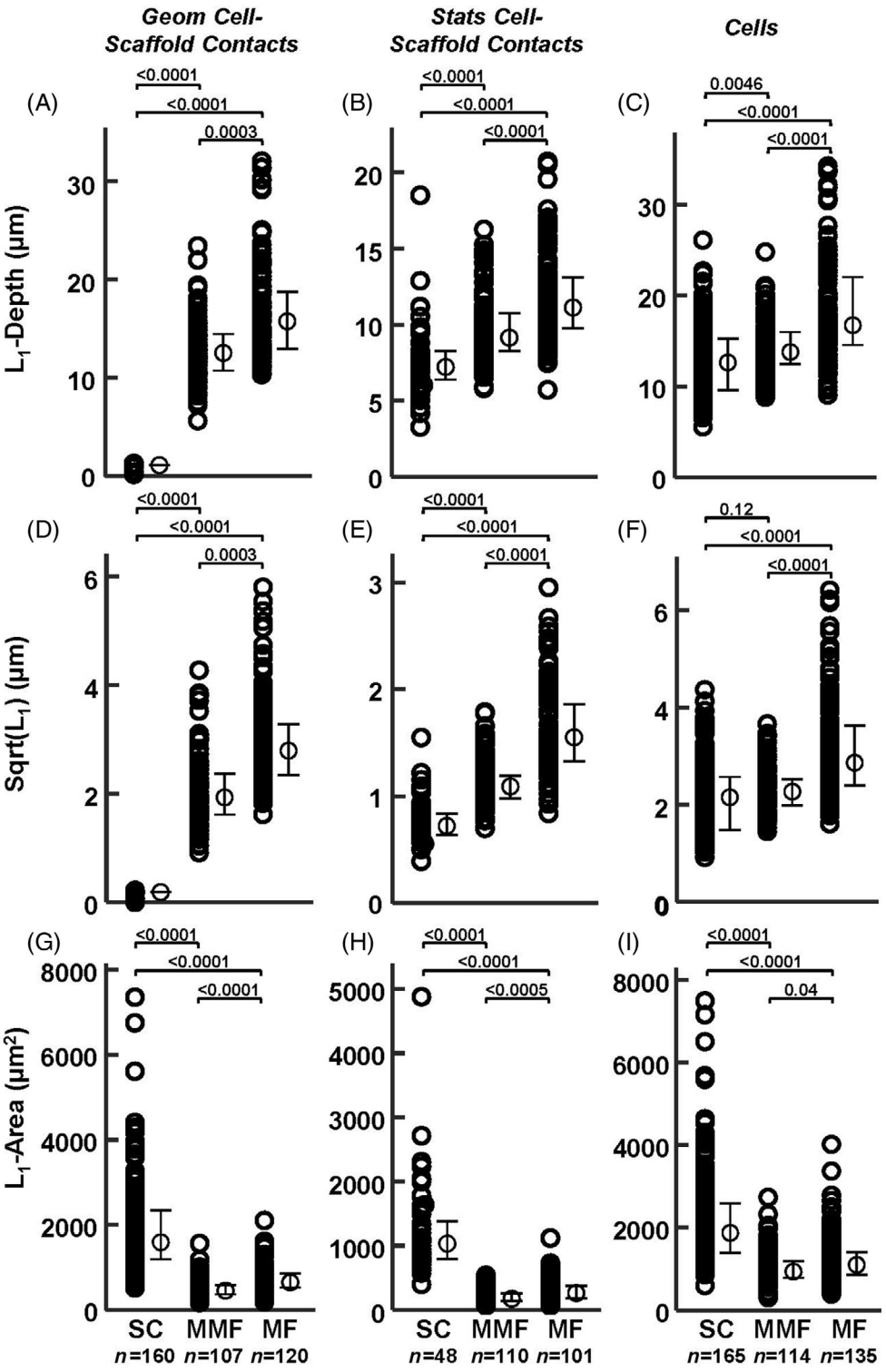

FIGURE 4 Plots of shape metrics for cell-scaffold contacts and cells. For each treatment, the individual data points are on the left, and the median with first and third quartiles are to the right. Above each plot are *p*-values for significance from the pairwise comparisons for Kruskal-Wallis non-parametric test using Dunn's multiple comparisons (with Sidak's correction for multiple comparisons)

surface roughness for SC was 52 nm (SD 32 nm), establishing that the SC films were essentially flat and planar with regard to MMF and MF.

3D visualizations of cells, scaffolds and cell-scaffold contacts are shown for the Geom analysis (Figure 3) and Stats analysis (Figure S1). The three channels for each scaffold (SC, MMF, MF) are shown in seven different combinations to show how the cells interacted with the fibers (MF and MMF) and the film (SC). The red channel shows the cell-scaffold contacts, which are the pixels that lie at the interface between the cell and the substrate (SC, MMF, MF). The cell-scaffold contacts for SC were planar, demonstrating how the cell-scaffold contacts were confined to basal surface of the cells cultured on SC flat films. The cell-scaffold contacts for fibers (MMF, MF) were in many planes in 3D space over the cell surface. Cells on fibers had extensions that followed along the fibers and penetrated down into the fiber mat by two or three fiber layers. Similar morphologies for the cell-scaffold contacts were observed for the two different analytical approaches

(Geom [Figure 3] and Stats [Figure S1]), improving confidence in these results.

The shape dimensionality analysis results for cells, Geom-cell-scaffold contacts and Stats-cell-scaffold contacts are shown in Figure 4. The L_1-Depth is the caliper length of the shortest axis of the 3D point cloud and is a measure of dimensionality where a larger L_1-Depth indicates greater 3D character. Cells cultured on fiber scaffolds (MF and MMF) had a larger L_1-Depth than cells cultured on flat surfaces (SC) (Figure 4A,B). In addition, the L_1-Depth of cell-scaffold contacts was larger for cells cultured on fiber scaffolds (MF and MMF) than on flatter surface (SC) as measured by both the Geom analyses (Figure 4A) and Stats analyses (Figure 4B). Generally, the L_1-axis is mostly perpendicular to the plane of the culture substrate, but not completely.

Sqrt(L_1) was larger for cells and cell-scaffold contacts cultured on MF and MMF than for cells cultured on SC (Figure 4D–F). Sqrt(L_1) is another measure of an object's dimensionality where a larger value indicates greater dimensionality and a more 3D shape. Statistical testing indicated that differences between SC, MMF, and MF for the L_1-Depth and Sqrt(L_1) for the cells and cell-scaffold contacts were statistically significant in nearly all cases for both the Geom and Stats analyses (Figure 4 and Figure S3).

Both L_1-Depth and Sqrt(L_1) increased in size from SC to MMF to MF, indicating that the overall shape of cells and their scaffold contacts had the flattest profile on the planar SC films and had a thicker, more 3D profile on the fiber scaffolds. The general agreement between the results for L_1-Depth and Sqrt(L_1), which are similar but not mathematically the same, improves the confidence in results.

Many additional cell and cell-scaffold contact shape metrics are given in the supplemental information (Figure S2). The L_2-Aspect Ratio and L_3-Aspect Ratio also demonstrate greater cell-scaffold contact dimensionality for MMF and MF than for SC. The L_2-Aspect Ratio is a bounding box aspect ratio computed from the maximum intensity projection of the cell-scaffold contacts along the L_2-axis (L_1-axis is shortest, L_2- axis is the middle, L_3-axis is longest). L_2-Aspect Ratio is larger for objects with lower dimensionality since the object's minimum depth, which goes in the denominator (aspect ratio = larger dimension divided by smaller dimension), is thinner. Cell-scaffold contacts for SC have a smaller minimum depth than MMF and MF, which causes SC to have the largest L_2-Aspect Ratio for both the Geom and

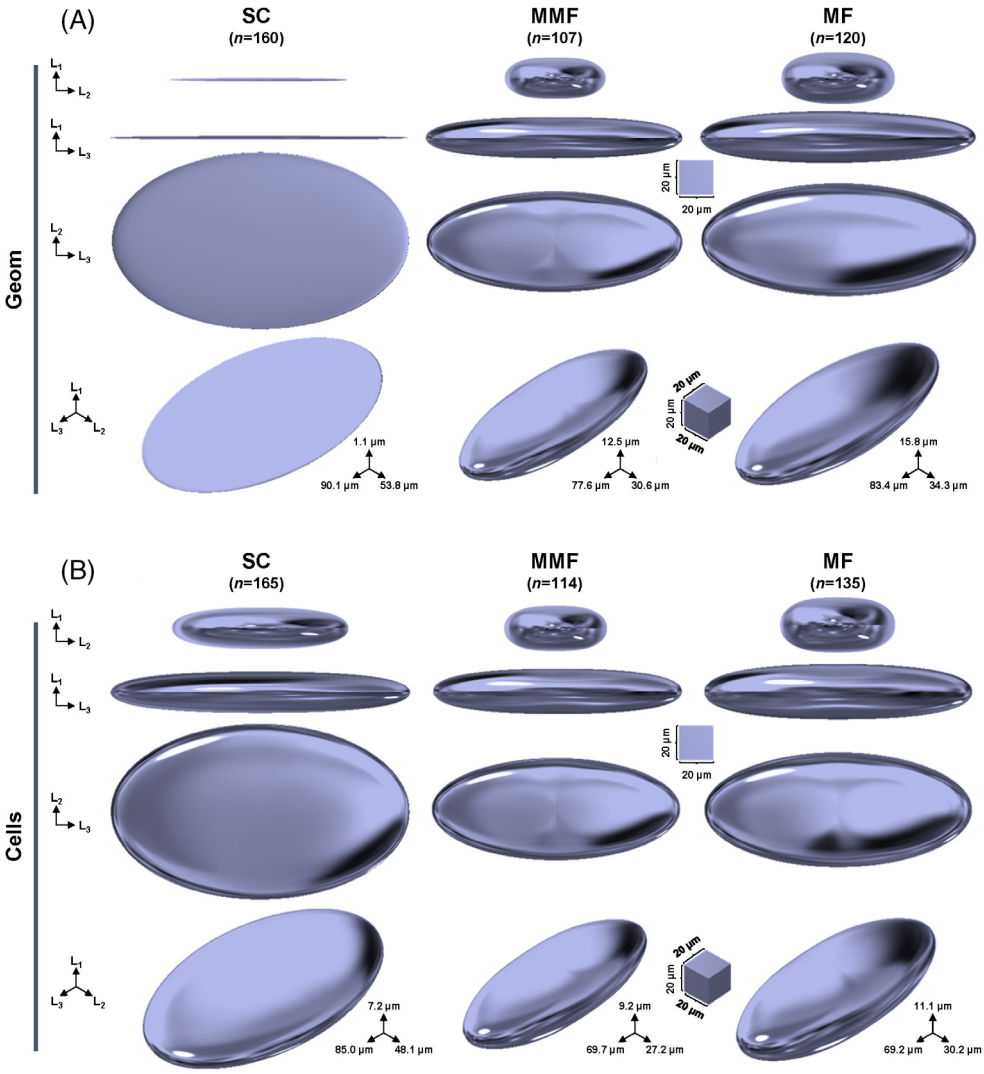

FIGURE 5 Ellipsoids were created for visualizing the dimensionality of the cell-scaffold contacts and cells (Geom analysis). The mean L_1-depth, L_2-Depth, and L_3-Depth were used as the lengths of the three ellipsoid axes. The ellipsoids are shown from four different views and the directions of the axes are given to the left. A size bar in the form of a square is given for the top three rows of each panel. The bottom row of each panel is an orthographic view, has the length of the axes shown along the bottom and has an orthographic size cube that applies only to the orthographic ellipsoids

Stats analyses. Likewise, the L_3-Aspect Ratio, which is the bounding box aspect ratio along the L_3-axis, is also largest for the SC cell-scaffold contacts for both the Geom and Stats analyses. Thus, results for 4 different dimensionality metrics (L_1-Depth, Sqrt(L_1), L_2-Aspect Ratio, L_3-Aspect Ratio) as computed by two different analytical methods (Geom, Stats) indicate that cell-scaffold contacts are larger for fiber scaffolds (MMF, MF) than for planar films (SC).

Ellipsoid visualizations of the cells and cell-scaffold contacts were created using computer-aided design software (Figure 5 and Figure S4). The mean L_1-Depth, L_2-Depth and L_3-Depth were used as the lengths of the ellipsoid axes. The ellipsoid renderings are shown from several points of view so that the viewer can better appreciate their shape and dimensionality. When looking at the Geom-cell-film contacts down the L_3-axis or L_2-axis (L_1-axis is vertical on the page), the contacts for SC are flat and thin (Figure 5A). In contrast, the cell-scaffold contacts for MMF and MF are thicker along the L_1-axis as the cell extends along the fibers into multiple planes and occupies a greater volume along the shortest axis. These results are corroborated by the Stats analysis of the cell-scaffold contacts (Figure S4), although the flatness of the SC contacts is not as pronounced due to differences in the contact point calculation method. However, the greater thickness of the cell-scaffold contacts along the L_1-axis is still apparent for MMF and, especially, MF. When looking at the cell ellipsoids down the L_3-axis or L_2-axis (Figure 5B), where the L_1 axis runs vertically along the page, the cells on SC are slightly thinner than MMF along L_1-axis. However, cells on MF appear thicker along the L_1-axis as they extend along the larger fibers and take on a shape with greater dimensionality.

A final measurement to be discussed is the cell-scaffold adhesion area, which is considered here as an infinitely thin surface with no volume that may undulate over the surface of the scaffold and indicates the areas where the cell is in contact with the scaffold. Within the domain of a 3D image, the cell-scaffold contact area would be represented by a surface (or surfaces) with a thickness of 1 pixel. For fibers, the cell-scaffold contact areas may be multiple objects that are not in contact with one another, since the cell may be in contact with many fibers that are not touching. Of the shape metrics that have been measured, the L_1-Area metric, which is the "area of the maximum intensity projection looking down the L_1-axis" (Table S1), is best for the assessment of the cell-scaffold contact area. The L_1-Axis is aligned with the shortest axis of the cell-scaffold contact volumes, such that the view down this axis presents the largest possible view of the cell-scaffold contact volumes, where the L_2-Axis (middle-length axis) and L_3-Axis (longest axis) are perpendicular to one another.

The Surface Area metric was not used to assess "cell-scaffold adhesion area," since Surface Area may overestimate the adhesion area. This is because the Surface Area metric treats the contacts as a volume, and the Surface Area of the volume would include the top area, bottom area and all four sides of the volume. In contrast, a maximum intensity projection of an object will only include the area from the side of the object that is being viewed. Thus, L_1-Area is the best indicator of the size of the cell-scaffold adhesion area. L_1-Area of cell-scaffold contacts was larger for SC than for MMF and MF, as determined by both the Geom and Stats analyses (Figure 4). The size of cell-scaffold contacts can affect cell adhesive strength and cell-adhesion-mediated signaling.

4 | DISCUSSION

The dimensionality of cell-scaffold contacts was determined by 3D imaging and analysis. Due to the challenges of 3D image analysis,[33,34] two approaches were used for scaffold segmentation: "Geom" and "Stats." Geom is a geometrical model where the scaffold fibers (MF and MMF) were modeled as cylinders and the flat films (SC) were modeled as planes. In contrast, Stats is a statistical model that used the voxel intensities of the scaffold channel to generate probabilities that were used to determine which voxels should be assigned as scaffold. For both models (Geom and Stats), the cell-scaffold contacts were determined by adjacency or co-occurrence of cell and scaffold voxels. The Geom and Stats approaches are based on fundamentally different principles which have different biases and interferences so that using them together may improve the confidence in the results.

The strength of the Geom analysis is that it forces the scaffold imaging data to fit into predefined shapes (cylinders for MMF and MF and planes for SC). This makes sense in light of the a priori knowledge from SEM and AFM (Figure 1) that MMF and MF are cylindrical fibers and that SC are planar substrates. The weakness of this approach is that it may not detect artifacts or anomalies in the data. For example, a sample could be damaged, the imaging data could be distorted by an obstruction in the light path (dust, debris), or the shape of the substrates (SC, MMF, MF) may deviate from what is expected, and the Geom models would still try to force the results to fit into cylinders (MMF, MF) and planes (SC).

The strength of the statistical model is that it does not make any assumptions about the shape of the samples. It does not assume that the fibers (MMF, MF) are cylindrical or that films (SC) are planar. If the shapes of SC, MMF or MF deviate from what is expected, then this will be reflected in the results. The weakness of this approach is that it does not capitalize on the a priori knowledge that MMF and MF are cylindrical fibers and that SC is planar (Figure 1). Using confocal to image fibers, which are a few micrometers in size, and cells, which have features that are a few micrometers in size, pushes the limits of the confocal resolution. This leads to data with lower signal to noise ratio that is challenging to segment, which is why it may be helpful to utilize the a priori knowledge that fibers are cylindrical and films are planar.

Using the Stats and Geom analyses together enables a better assessment of the reliability of the results. When the results from the two models agree, then there is greater confidence in the results. When the results from the two analyses do not agree, the reliability of the results may be more carefully considered. There may be reasons why one or the other model could be more reliable for a particular substrate or shape metric, or maybe the results are not reliable.

The trends for the dimensionality metrics as determined by the Geom and Stats analyses were similar. For both analyses, four metrics

of dimensionality (L_1-Depth, Sqrt(L_1), L_2-Aspect Ratio and L_3-Aspect Ratio) demonstrated an increase in the 3D nature of cell-scaffold contacts from flat films (SC) to medium-sized fibers (MMF) to larger-sized fibers (MF). These trends were observed for both the cell-scaffold contact shape measurements (Figure 4A,B,D,E) and for the cell shape measurements (Figure 4C,F). In addition, the size of the cell-scaffold contact area (L_1-Area) was larger for SC than for fibers (MMF, MF).

These results have implications for intracellular signal transduction. Since cell adhesion sites are a well-known source of intracellular signaling,[5,35] the observations that cells in 3D scaffolds (MMF and MF) make contacts with the scaffold in multiple planes over the surface of the cell indicate that adhesion-site initiated signaling could emanate from multiple planes over the surface of the cell. In contrast, hBMSCs on SC made contact with their substrate along their bottom surface such that adhesion-site initiated signaling would emanate only from the bottom surface of the cells. In addition, the area of cell-scaffold contact was larger for cells in MMF and MF fiber scaffolds than for cells on the planar SC surfaces. The differences in the dimensionality, geometry, and size of the cell-scaffold contacts for fibers versus films could affect the adhesion-mediated signaling[16,17,25,26] that influences cell behaviors such as proliferation, differentiation, and apoptosis.

The current 3D data set of cell-scaffold contacts could be useful for biochemical signaling simulations.[25,26,36] Simulations could assess how signaling kinetics may differ for the flattened cells in SC, whose adhesion-site initiated signaling emanates from their bottom surface, versus cells in MMF and MF with greater 3D character whose adhesion-site initiated signaling emanates from multiple locations over the surface of the cell.

In addition, the approaches developed herein could be useful to future studies. The method for imaging the scaffolds by spiking them with fluors could be used for comparing cell niches in other types of scaffolds, such as freeform fabricated or melt electrowritten scaffolds. The three key metrics used herein, L_1-Depth, Sqrt(L_1), and L_1-Area, are useful for comparing the dimensionality and area of the cell-scaffold contacts within cells niches of different scaffolds. In addition, other 3D imaging studies of scaffolds, cell shape and cell-scaffold contacts can improve confidence in results by using two or more segmentation algorithms that are based on different principles. Herein, the Stats analysis did not use a priori knowledge of scaffold structure for segmentation while Geom analysis capitalized on the a priori knowledge that SC films are planar and that MMF and MF fibers are cylindrical.

5 | CONCLUSIONS

The morphology and dimensionality of the cell-scaffold contacts made by hBMSCs during culture in electrospun polymeric fiber scaffolds have been measured by confocal fluorescence imaging and image analysis. Results were compared to the cell-substrate contacts made between hBMSCs and flat polymer films. Two methods based on fundamentally different principles, geometrical assumptions versus statistical assumptions, were used to analyze the imaging data. Results indicated that cells cultured in fiber-based scaffolds assumed morphologies with greater 3D character and made contact with the fibers in multiple planes over the cell surface. In contrast, cells cultured on flat films took on flatter morphologies and made contact with the substrate only along their bottom surface. These results have implications for intracellular signaling cascades that originate at cell adhesion sites. For cells in 3D scaffolds, adhesion-mediated signaling events may initiate from many different planes over the surface of the cells, while adhesion-mediated signaling may only originate from the bottom surface of cells cultured on planar surfaces. These differences in the geometry of cell-adhesion sites for cells in fiber-based scaffolds versus planar films may influence second messenger signaling kinetics leading to changes in cell functions such as proliferation, differentiation, and apoptosis.

ACKNOWLEDGMENTS

Stephanie J. Florczyk and Nathan A. Hotaling were supported by National Institute of Standards and Technology - National Research Council Research Associateships. Allison L. Horenberg was supported by the National Institute of Standards and Technology Summer Undergraduate Research Fellowship. We thank Sowon Yoon for assistance with the image analysis. The hBMSCs employed in this work were obtained from the Tulane Center for Gene Therapy (NCRR-NIH P40RR017447). The "standard deviation" (SD) is the same as the "combined standard uncertainty of the mean" for the purposes of this work. This article, a contribution of NIST, is not subject to US copyright. Certain equipment and instruments or materials are identified in the article to adequately specify the experimental details. Such identification does not imply recommendation by NIST, nor does it imply the materials are necessarily the best available for the purpose.

FUNDING INFORMATION

The authors received no specific funding for this work.

CONFLICT OF INTEREST

The authors declare that no competing interests exist.

DATA AVAILABILITY STATEMENT

All relevant data are within the paper, its Supporting Information files and posted on the web at the links indicated within the manuscript.

REFERENCES

1. Hoggatt J, Scadden DT. The stem cell niche: tissue physiology at a single cell level. *J Clin Invest*. 2012;122:3029-3034. doi:10.1172/JCI60238
2. Schlaepfer DD, Hauck CR, Sieg DJ. Signaling through focal adhesion kinase. *Prog Biophys Mol Biol*. 1999;71:435-478. doi:10.1016/s0079-6107(98)00052-2
3. Schneider GB, Zaharias R, Stanford C. Osteoblast integrin adhesion and signaling regulate mineralization. *J Dent Res*. 2001;80:1540-1544.
4. Tan SJ, Chang AC, Anderson SM, et al. Regulation and dynamics of force transmission at individual cell-matrix adhesion bonds. *Sci Adv*. 2020;6:eaax0317. doi:10.1126/sciadv.aax0317

5. Gahmberg CG, Grönholm M. How integrin phosphorylations regulate cell adhesion and signaling. *Trends Biochem Sci*. 2022;47:265-278. doi:10.1016/j.tibs.2021.11.003
6. Murphy WL, McDevitt TC, Engler AJ. Materials as stem cell regulators. *Nat Mater*. 2014;13:547-557. doi:10.1038/nmat3937
7. Bianco P, Robey PG. Skeletal stem cells. *Development*. 2015;142:1023-1027. doi:10.1242/dev.102210
8. Ruckh TT, Kumar K, Kipper MJ, Popat KC. Osteogenic differentiation of bone marrow stromal cells on poly(epsilon-caprolactone) nanofiber scaffolds. *Acta Biomater*. 2010;6:2949-2959. doi:10.1016/j.actbio.2010.02.006
9. Kumar G, Tison CK, Chatterjee K, et al. The determination of stem cell fate by 3D scaffold structures through the control of cell shape. *Biomaterials*. 2011;32:9188-9196. doi:10.1016/j.biomaterials.2011.08.054
10. Folkman J, Moscona A. Role of cell shape in growth control. *Nature*. 1978;273:345-349. doi:10.1038/273345a0
11. Chen CS, Mrksich M, Huang S, Whitesides GM, Ingber DE. Geometric control of cell life and death. *Science*. 1997;276:1425-1428. doi:10.1126/science.276.5317.1425
12. Cukierman E, Pankov R, Stevens DR, Yamada KM. Taking cell-matrix adhesions to the third dimension. *Science*. 2001;294:1708-1712. doi:10.1126/science.1064829
13. Weiss P, Garber B. Shape and movement of mesenchyme cells as functions of the physical structure of the medium: contributions to a quantitative morphology. *Proc Natl Acad Sci U S A*. 1952;38:264-280. doi:10.1073/pnas.38.3.264
14. Farooque TM, Camp CH, Tison CK, Kumar G, Parekh SH, Simon CG. Measuring stem cell dimensionality in tissue scaffolds. *Biomaterials*. 2014;35:2558-2567. doi:10.1016/j.biomaterials.2013.12.092
15. Florczyk SJ, Simon M, Juba D, et al. A bioinformatics 3D cellular morphotyping strategy for assessing biomaterial scaffold niches. *ACS Biomater Sci Eng*. 2017;3:2302-2313. doi:10.1021/acsbiomaterials.7b00473
16. Gallant ND, Michael KE, García AJ. Cell adhesion strengthening: contributions of adhesive area, integrin binding, and focal adhesion assembly. *Mol Biol Cell*. 2005;16:4329-4340. doi:10.1091/mbc.e05-02-0170
17. Elineni KK, Gallant ND. Regulation of cell adhesion strength by peripheral focal adhesion distribution. *Biophys J*. 2011;101:2903-2911. doi:10.1016/j.bpj.2011.11.013
18. Cavalier-Smith T. Nuclear volume control by nucleoskeletal DNA, selection for cell volume and cell growth rate, and the solution of the DNA C-value paradox. *J Cell Sci*. 1978;34:247-278. doi:10.1242/jcs.34.1.247
19. Tutak W, Jyotsnendu G, Bajcsy P, Simon CG. Nanofiber scaffolds influence organelle structure and function in bone marrow stromal cells. *J Biomed Mater Res B Appl Biomater*. 2017;105:989-1001. doi:10.1002/jbm.b.33624
20. Bidwell JP, Alvarez M, Feister H, Onyia J, Hock J. Nuclear matrix proteins and osteoblast gene expression. *J Bone Miner Res*. 1998;13:155-167. doi:10.1359/jbmr.1998.13.2.155
21. McNamara LE, Burchmore R, Riehle MO, et al. The role of microtopography in cellular mechanotransduction. *Biomaterials*. 2012;33:2835-2847. doi:10.1016/j.biomaterials.2011.11.047
22. Chambliss AB, Khatau SB, Erdenberger N, et al. The LINC-anchored Actin cap connects the extracellular milieu to the nucleus for ultrafast mechanotransduction. *Sci Rep*. 2013;3:1087. doi:10.1038/srep01087
23. Lizana L, Bauer B, Orwar O. Controlling the rates of biochemical reactions and signaling networks by shape and volume changes. *Proc Natl Acad Sci USA*. 2008;105:4099-4104. doi:10.1073/pnas.0709932105
24. Chan Y-HM, Marshall WF. Scaling properties of cell and organelle size. *Organogenesis*. 2010;6:88-96. doi:10.4161/org.6.2.11464
25. Meyers J, Craig J, Odde DJ. Potential for control of signaling pathways via cell size and shape. *Curr Biol CB*. 2006;16:1685-1693. doi:10.1016/j.cub.2006.07.056
26. Rangamani P, Lipshtat A, Azeloglu EU, et al. Decoding information in cell shape. *Cell*. 2013;154:1356-1369. doi:10.1016/j.cell.2013.08.026
27. Hotaling NA, Bharti K, Kriel H, Simon CG. DiameterJ: a validated open source nanofiber diameter measurement tool. *Biomaterials*. 2015;61:327-338. doi:10.1016/j.biomaterials.2015.05.015
28. Cole RW, Jinadasa T, Brown CM. Measuring and interpreting point spread functions to determine confocal microscope resolution and ensure quality control. *Nat Protoc*. 2011;6:1929-1941. doi:10.1038/nprot.2011.407
29. Bajcsy P, Yoon S, Florczyk SJ, et al. Modeling, validation and verification of three-dimensional cell-scaffold contacts from terabyte-sized images. *BMC Bioinform*. 2017;18:526. doi:10.1186/s12859-017-1928-x
30. Bajcsy P, Simon M, Florczyk SJ, Simon CG, Juba D, Brady MC. A method for the evaluation of thousands of automated 3D stem cell segmentations. *J Microsc*. 2015;260:363-376. doi:10.1111/jmi.12303
31. Bajcsy P. Web cell segmentation and cell-scaffold contact verification. National Institute of Standards & Technology (web page), 2017. https://isg.nist.gov/deepzoomweb/stemcells3dcontact/index.html.
32. Simon Jr CG, Bajcsy P. Data set: cell-scaffold contact (web page), 2017. doi: 10.18434/M31824
33. Bajcsy P, Cardone A, Chalfoun J, et al. Survey statistics of automated segmentations applied to optical imaging of mammalian cells. *BMC Bioinform*. 2015;16:330. doi:10.1186/s12859-015-0762-2
34. Reznikov N, Buss DJ, Provencher B, McKee MD, Piché N. Deep learning for 3D imaging and image analysis in biomineralization research. *J Struct Biol*. 2020;212:107598. doi:10.1016/j.jsb.2020.107598
35. Romani P, Valcarcel-Jimenez L, Frezza C, Dupont S. Crosstalk between mechanotransduction and metabolism. *Nat Rev Mol Cell Biol*. 2021;22:22-38. doi:10.1038/s41580-020-00306-w
36. Betancourt BAP, Florczyk SJ, Simon M, et al. Effect of the scaffold microenvironment on cell polarizability and capacitance determined by probabilistic computations. *Biomed Mater Bristol Engl*. 2018;13:025012. doi:10.1088/1748-605X/aa9650

SUPPORTING INFORMATION

Additional supporting information can be found online in the Supporting Information section at the end of this article.

How to cite this article: Florczyk SJ, Hotaling NA, Simon M, et al. Measuring dimensionality of cell-scaffold contacts of primary human bone marrow stromal cells cultured on electrospun fiber scaffolds. *J Biomed Mater Res*. 2023;111(1):106-117. doi:10.1002/jbm.a.37449